

## RESEARCH ARTICLE

# The Effects of Partial Shading on a Grid-Integrated Photovoltaic System with MATLAB-SIMULINK

Farhanur Rahman<sup>1</sup>, Mohammad Jarif Bulbul<sup>1</sup>, Minhaz Yeamin<sup>1</sup>, Arif Ahammad<sup>2</sup>

<sup>1</sup>Department of EEE, Sylhet Engineering College, Shahjalal University of Science and Technology, Sylhet, Bangladesh

<sup>2</sup>Department of EEE, Shahjalal University of Science and Technology, Sylhet, Bangladesh

**Cite this article as:** F. Rahman, M. Jarif Bulbul, M. Yeamin and A. Ahammad, "The effects of partial shading on a grid-integrated photovoltaic system with MATLAB-SIMULINK," *Turk J Electr Power Energy Syst.*, 2025; 5(1), 66-77.

## ABSTRACT

Photovoltaic (PV) technology has gained significant popularity in recent years. While integrating solar energy into power systems offers numerous benefits, it can also lead to challenges such as voltage instability, increased total harmonic distortion, and power quality issues, especially under partial shading conditions (PSC). These conditions can result in multiple local maximum power points on the power–voltage (P–V) curve. To address these challenges, maximum power point tracking controllers are essential for maximizing power output from PV systems. This study presents the successful implementation of a three-phase, grid-integrated PV system in various scenarios, including PSC, standard test conditions, and variations in load. The implementation achieved some impressive results in mitigating the instabilities. The proposed strategy was simulated and evaluated using the MATLAB/Simulink environment.

**Index Terms**—Grid-integrated PV systems, modeling, partial shading conditions, solar irradiation, total harmonic distortion (THD)

## I. INTRODUCTION

Globally, experts are actively exploring alternative approaches to reduce energy costs and mitigate greenhouse gas emissions through the adoption of clean and renewable energy sources. Integrating these sources into power generation systems is considered the most optimal approach for enhancing the current situation, given their superior attributes compared to other energy sources [1]. Due to characteristics like lower production costs, lack of carbon emissions, and competitive pricing, renewable energy is gaining popularity as an alternative to conventional power generation [2]. By 2030, the production of renewable energy is expected to rise by 6.7% [3]. According to ref. [4], as of early 2024, the global solar power capacity had surpassed 1 terawatt (TW). Consequently, 133.7 billion USD, or 55% of the total cost of renewable energy, was invested in the production of photovoltaic (PV) energy in 2016 [5]. Photovoltaic energy resources have emerged as the leading alternative for electricity generation among various renewable energy sources, especially in unpredictable weather conditions. Nurunnabi et al. [1] highlighted the potential of grid-tied hybrid renewable energy systems in reducing energy costs and emissions. The significant decrease in the price of PV modules, coupled with the rising demand for renewable

energy systems, has led to the development of large-scale PV power plants in several countries worldwide. However, ensuring the optimal performance of individual PV panels within an array becomes crucial as they are exposed to various environmental situations. The increasing adoption of solar energy presents new technical challenges due to its variable nature, as solar power is not consistent and depends on factors like weather and other environmental conditions [6]. Photovoltaic modules are designed to convert solar energy into electrical energy. They consist of interconnected PV cells that generate both voltage and electric current, which can be utilized for practical applications. Additionally, these modules are structured to ensure proper cell protection and form a cohesive unit. According to ref. [7], the energy conversion efficiency of the most advanced solar cells, made of monocrystalline silicon and manufactured in laboratories, is around 25%. This efficiency rate is relatively low compared to other forms of energy generation currently in use. Batteries are used in standalone PV systems to store the energy generated from solar panels, providing an independent power supply. Conversely, grid integration of PV does not require a battery storage system, making it a financially feasible solution [8]. According to ref. [9], by 2050, solar PV energy sources, with an installed capacity of 4600 GW, will

**Corresponding Author:** Arif Ahammad, arif-eee@sust.edu



Content of this journal is licensed under a Creative Commons Attribution (CC BY) 4.0 International License.

**Received:** July 2, 2024  
**Revision requested:** November 18, 2024  
**Last revision received:** October 30, 2024  
**Accepted:** November 18, 2024  
**Publication Date:** January 20, 2025

be responsible for up to 16% of global energy consumption. Despite the numerous benefits of renewable energy, their integration into the power grid can pose challenges. The inconsistent nature of solar power can result in voltage instability, increased total harmonic distortion (THD), and other power quality problems. These issues can significantly impact the overall performance and reliability of the electrical grid [10, 11, 12, 13]. Power electronic technology plays a crucial role in effectively interconnecting renewable energy sources with the grid network to address this issue. Currently, the majority of PV installations employ Maximum Power Point Tracking (MPPT) control, which can cause variations in output energy due to alterations in irradiance intensity and different environmental considerations. Additionally, electrical constraints and system control can further contribute to differences in output energy [14]. The typical approach to achieve MPPT involves employing a direct current (DC)–DC Boost converter that connects the PV array to the inverter. The goal is to generate more energy by improving the efficiency of the solar panel through optimizing the performance of the PV array [15]. Rahman et al.'s [16] LLC resonant DC–DC boost converter achieved 98.4% peak efficiency but with higher ripple voltage. Our single-switch cascaded DC–DC boost converter, employed to interface PV arrays with the inverter and equipped with an MPPT controller, achieved a slightly lower efficiency of 94% but exhibited lower ripple. This indicates a potential compromise between efficiency and ripple in these converter types. In conditions of consistent irradiance, the power–voltage (P–V) characteristics of a PV system only demonstrate a single curve [17]. In such scenarios, the Perturb and Observe (P&O) and Incremental Conductance (INC) algorithms are commonly used for MPPT. These algorithms strike a balance between performance and simplicity. While other conventional MPPT algorithms show effective performance in uniformly irradiated PV setups, their efficiency tends to be significantly impacted when operating in partial shading conditions (PSC). This is attributed to the tendency of MPPT techniques to often converge to the local maximum power point (LMPP) rather than the global maximum power point (GMPP) [18]. The state-space analysis method is a commonly employed technique

for evaluating the stability of grid-connected systems. This method involves constructing a state-space model of the system and evaluating its stability by analyzing the eigenvalues in the complex plane. State-space analysis provides a means to assess the stability of grid-connected PV systems under varying solar irradiance. Nevertheless, verifying state-space models can be intricate, particularly for large and complex systems, as deriving analytical models becomes quite challenging

Nevertheless, verifying state-space models can be intricate, particularly for large and complex systems, as deriving analytical models becomes quite challenging. In this study, a simulation analysis of the impact on a grid-connected PV system under PSC is presented with a power rating of 400 kilowatts peak (kWp). To make the output voltage and current free of any steady-state error, PI controllers are utilized, and their outputs are subsequently transmitted through a P&O algorithm to control the duty cycle of the DC–DC converter. A three-phase voltage source converter (VSC) inverter is employed between the DC–DC converter and the utility grid to generate a sinusoidal grid current operating at a frequency of 60 Hz.

## II. CONFIGURATION OF THE GRID-INTEGRATED PV SYSTEM

### A. PV Array

A PV array (Fig. 1) is a system composed of multiple interconnected solar panels designed to harness sunlight and convert it into usable electricity. These solar panels consist of PV cells made from semiconductor materials that generate DC electricity when exposed to sunlight. The PV array's efficiency and output depend on factors such as the quality of the solar panels, their orientation, tilt angle, and the amount of sunlight they receive [19, 20].

The equation used to calculate the terminal current ( $I$ ) is given below:

$$I = I_{ph} - I_D - I_{sh} \quad (1)$$

where  $I_{ph}$  = photo current,  $I_D$  = diode current, and  $I_{sh}$  = shunt current.

The current given above is calculated by using the equation below:

$$I_{ph} = \frac{(I_{sc} + (K_i(T - T_{ref}))) * L}{1000} \quad (2)$$

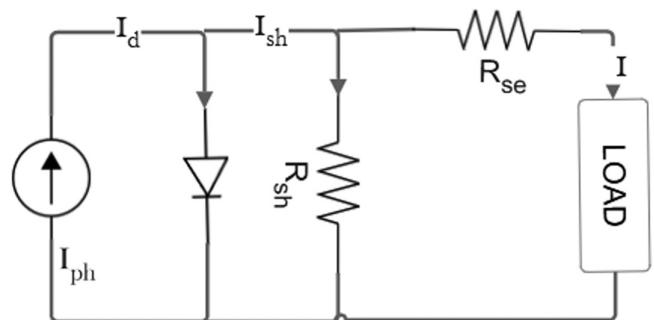


Fig. 1. Diagram of PV array.

### Main Points

- The study focuses on how partial shading affects the system's performance, i.e., the power quality challenges faced by photovoltaic (PV) systems under partial shading conditions (PSC), which can lead to multiple local maximum power points and a global maximum power point on the power–voltage curve.
- The research highlights the importance of maximum power point tracking controllers for optimizing power output from PV systems under various environmental conditions, including PSC. PI controllers are used to regulate the output voltage and current, and a P&O algorithm controls the DC–DC converter for optimal power output.
- Results of a simulation of a three-phase VSC inverter that converts the DC output to a 60 Hz sinusoidal current for feeding the utility grid conducted using MATLAB/Simulink to analyze the system's performance under different scenarios, including PSC and standard test conditions.

where  $I_{sc}$  = short circuit current,  $K_i$  = coefficient of short circuit current (A/°C),  $T$  = variable temperature,  $T_{ref}$  = reference temperature (298 K), and  $L$  = solar irradiance (W/m<sup>2</sup>).

$$I_D = I_o \left( \exp \left( \left( \frac{V + IR_{se}}{AKTN_s} \right) q \right) - 1 \right) \quad (3)$$

where  $R_{se}$  = series resistance,  $V$  = terminal voltage,  $N_s$  = the number of series PV cells,  $q$  = charge ( $1.6 \times 10^{-19}$  C),  $A$  = diode ideality factor,  $K$  = Boltzmann constant, and  $I_o$  = saturation current.

$$I_{sh} = \frac{(V + IR_{se})}{R_{sh}} \quad (4)$$

Here,  $R_{sh}$  = shunt resistance.

The parameters for the single PV panel are given in Table I.

Module: SunPower SPR-315E-WHT-D.

Four separate panels were used in this PV system. These panels received mostly unequal irradiation during the simulation. The irradiation was stepped up and down and kept the same during various periods, considering unclear weather, bird droppings, dust, and tall surroundings. The Fig. 2 and Fig. 3 show each panel's exposure to sun light to understand the partially shaded condition used in the simulation test.

### B. DC–DC Boost Converter

In order to link the load to the PV source and extract the optimum amount of power from the source, the boost converter is used. Based on the state of the power switch, it has two operational modes that differentiate its performance. The boost converter's two operating modes are presented in Fig. 4 [21].

During the switch is in the on state difference of voltage and current is given in the equations 5 and 6:

$$\frac{di_l}{dt} = \frac{1}{L_b} (V_{pv} - V_{dc}) \quad (5)$$

$$\frac{dV_{dc}}{dt} = \frac{1}{C_{dc}} (i_l - i_{inv}) \quad (6)$$

**TABLE I.**  
PV PARAMETERS

Number of parallel strings	64
Series-connected modules per string	5
Maximum power (W)	315.072
Open circuit voltage $V_{oc}$ (V)	64.6
Short-circuit current $I_{sc}$ (A)	6.14
Voltage at maximum power point $V_{mp}$ (V)	54.7
Current at maximum power point $I_{mp}$ (A)	5.76

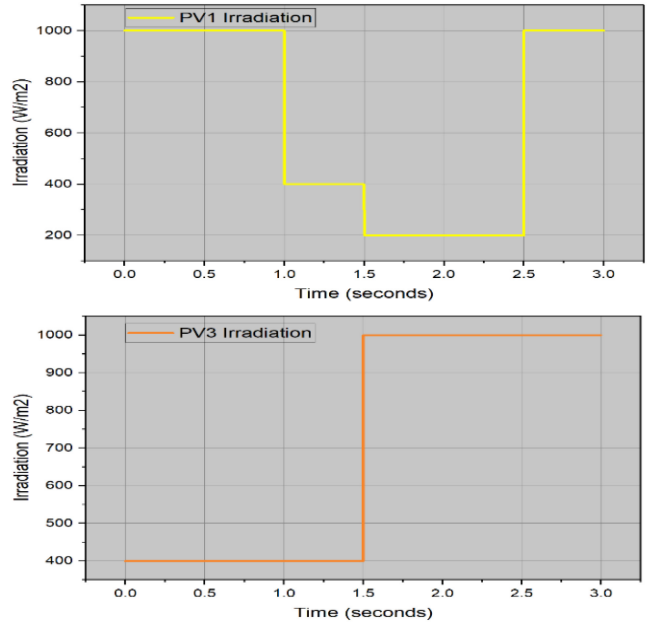


**Fig. 2.** Shading conditions for PV1 and PV3.

And during the switch's off state the difference of voltage and current has been shown in equations 7 and 8:

$$\frac{di_l}{dt} = \frac{1}{L_b} (V_{pv}) \quad (7)$$

$$\frac{dV_{dc}}{dt} = -\frac{1}{C_{dc}} (i_{inv}) \quad (8)$$

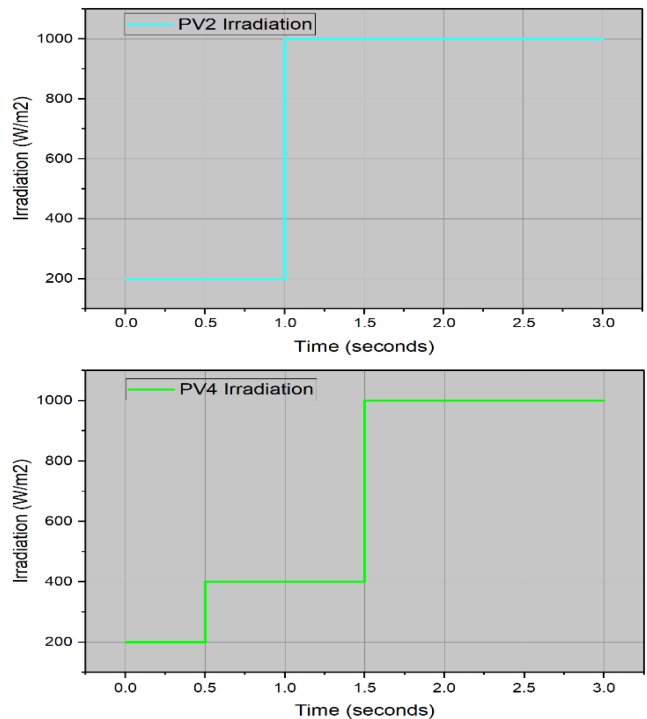


**Fig. 3.** Shading conditions for PV2 and PV4.

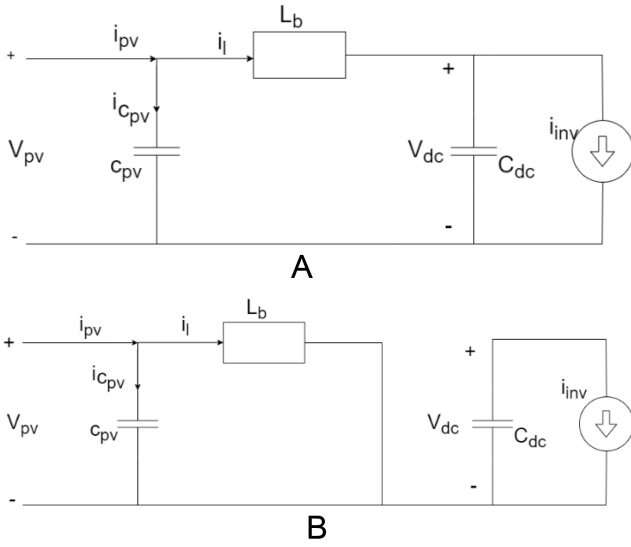


**Fig. 4.** Circuit of boost-converter when: (A) switch is off and (B) switch is on.

So here,  $i_l$  = inductor current,  $V_{dc}$  = capacitor voltage,  $L_b$  = boost converter inductance,  $I_{inv}$  = inverter current, and  $C_{dc}$  = coupling capacitor value (between the boost converter and the two-level inverter).

Employing the method of state space averaging, the boost model can be shown in the equations 9 and 10:

$$\mathbf{x} = \mathbf{A}\mathbf{x} + \mathbf{B}\mathbf{u} \quad (9)$$

$$\mathbf{y} = \mathbf{C}\mathbf{x} + \mathbf{D}\mathbf{u} \quad (10)$$

where  $\mathbf{x} = [i_{pv}, V_c]T$  is the state vector,  $\mathbf{u} = v_{pv}$  is the input voltage, and  $\mathbf{y} = v_c$  is the output voltage. Moreover  $\mathbf{A}$ ,  $\mathbf{B}$ ,  $\mathbf{C}$ , and  $\mathbf{D}$  are the system matrices and they can be presented as equation 11:

$$\mathbf{A} = \begin{bmatrix} 0 & -\frac{1-d}{L_b} & \frac{1-d}{C_{dc}} & 0 \\ \frac{1}{L_b} & -\frac{1}{C_{dc}} & 0 & 0 \end{bmatrix} \quad \mathbf{C} = [0 \ 1] \quad \mathbf{D} = [0] \quad (11)$$

Now here,  $L$  represents the inductance of the boost converter,  $C$  denotes the output capacitance of the boost converter,  $R$  stands for the load resistance, and  $d$  signifies the duty cycle.

The boost converter parameters are given in Table II.

**TABLE II.**  
BOOST CONVERTER PARAMETERS

Capacitance (C)	0.0001 F
Resistance (R)	0.005 Ohms
Inductance (L)	0.005 H
Sample Time (Ts)	0.00005 s

**C. DC-AC Control in Grid-Connected PV Inverters**

Fig. 5 demonstrates the VSC main controller for the inverter. There are two loops in the control system. They are an internal control loop and an external control loop. The internal control loop will regulate  $I_d$  and  $I_q$  grid currents. Here,  $I_d$  refers to components of active current, and  $I_q$  refers to the components of reactive current. Also, the external control loop will help to regulate the DC voltage of the inverter, and  $I_d$  reference current indicates the output for the DC voltage controller. To keep the P.F. at unity, the reference current  $I_q$  is set to 0. The current regulator voltage outputs,  $V_q$  and  $V_d$ , are converted to three-modulating signals ( $U_{ref-abc}$ ), which are utilized with the help of a pulse generator for three-level Pulse Width Modulation (PWM).

To synchronize the system inverter’s output AC voltage with the associated grid, PLL control is required. Here, the PLL type is called Discrete three-phase PLL. At the moment when the rotating reference frame aligns with the grid voltage and  $V_q$  becomes 0, the grid’s phase voltages are detected and converted to a space vector quantity. Thus, the PI controller sets the  $V_q$  to 0.

Here, Fig. 6 displays the PLL diagram, with the grid measurements ( $V$  and  $I$ ) in the d-q axis.

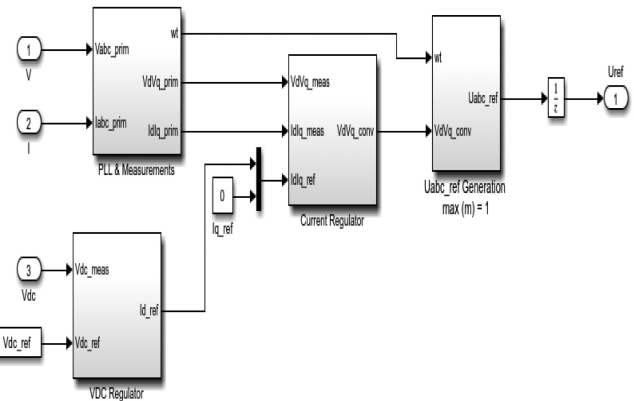


**Fig. 5.** Main controller for voltage source converter (VSC).

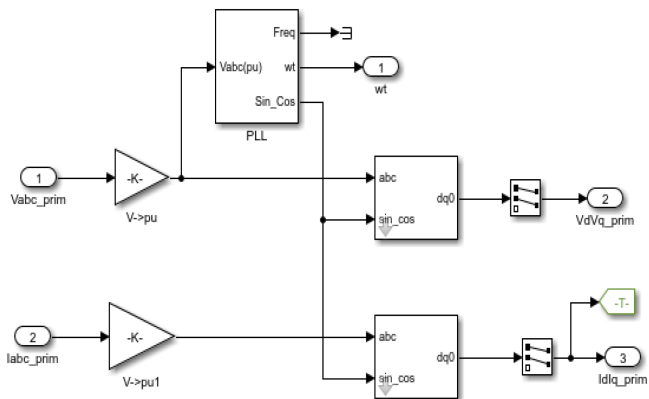


**Fig. 6.** PLL and grid measurements.

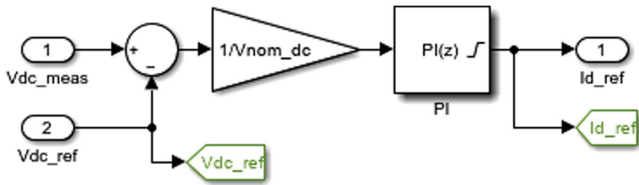


Fig. 7.  $V_{DC}$  regulator.

Fig. 7 shows the diagram of control loop for DC voltage in the three-phase inverter.

To regulate the commanded active and reactive power, current 4 control is used. The q and d-axis current loops are adjusted using the conventional PI controller, as illustrated in Fig. 8.

As shown in Fig. 9, the pulse generator for three-level PWM is used to modify the output voltages from the current regulator,  $V_q$  and  $V_d$ , to three modulating signals ( $U_{ref-abc}$ ) [22].

The comprehensive control diagram is illustrated in Fig. 10.

Parameters that had been used for the VSC inverter are given in Table III.

**D. Traditional P&O MPPT Technique**

Maximum Power Point Tracking is a strategy employed within solar PV systems with the aim of optimizing the power yield from solar panels. It involves the ongoing monitoring and adjustment of the operational point to align with the maximum power point (MPP) of the PV module or array. The MPPT algorithm functions by persistently observing the solar panel’s voltage and current while adapting the operational point to trace the MPP. This approach often integrates

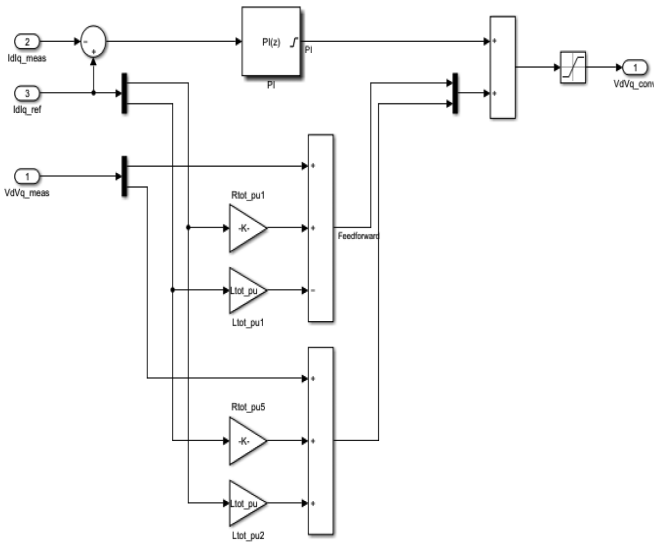


Fig. 8. Current controller block diagram.

a DC–DC converter positioned between the solar panel and the load or battery bank, enabling the transformation of the panel’s output voltage to the required level. Here’s a simplified explanation of how MPPT operates:

1. Measurement: The MPPT controller measures the solar panel’s voltage and current.
2. Power calculation: The controller determines the instantaneous power output of the solar panel from the calculated voltage and current.
3. Perturbation and observation: The MPPT controller slightly adjusts the operating point by either increasing or decreasing the panel’s output voltage or current. It observes how this adjustment affects the power output.
4. Comparison: The newly computed power output is compared with the previous power output. If the new power output is higher, the controller maintains the same adjustment direction. If it’s lower, the controller switches direction.
5. Iteration: Steps 2–4 are repeated at regular intervals to follow the MPP. The controller keeps adjusting the operating point until it either reaches the MPP or encounters specific limitations.

By continually tracking the MPP, MPPT controllers guarantee that solar panels function at their optimal efficiency, harnessing the most power possible from the panels amid changing environmental conditions. This optimization aids in elevating the energy harvest from the solar PV system, enhancing its overall performance.

**E. Power Diagram of Grid-Connected PV Array**

The power diagram for this grid-connected system is illustrated in Fig. 11.

The PV array is connected to a VSC inverter and is governed by a VSC control system that provides a  $U_{ref}$  signal to the inverter. After that, an LC filter is linked to it, and the grid system is activated. Transformers and other loads with three-phase sources make up the grid system. Two R-loads rated at 100 kW and 2 MW, along with an RLC-load of 2 MVA, can be seen connected. The transformer that is connected to the LC-filter side has a rating of 400 kVA, and the other one, which is at the source side, is 47 MVA. The three-phase source rating is 120 kV 2500 MVA.

**IV. RESULTS AND ANALYSIS**

Four different scenarios were taken into consideration for the analysis of the effect of PSC on the PV system by PSC and P&O MPPT algorithm application variations. They are:

1. With PSC and P&O algorithm.
2. Without PSC and with the P&O algorithm.
3. With PSC and without P&O.
4. Without PSC and P&O.

This study has analyzed the output parameters (i.e., power, voltage, and current) of the DC–DC boost converter and the voltage source inverter (VSI) under these four different conditions.

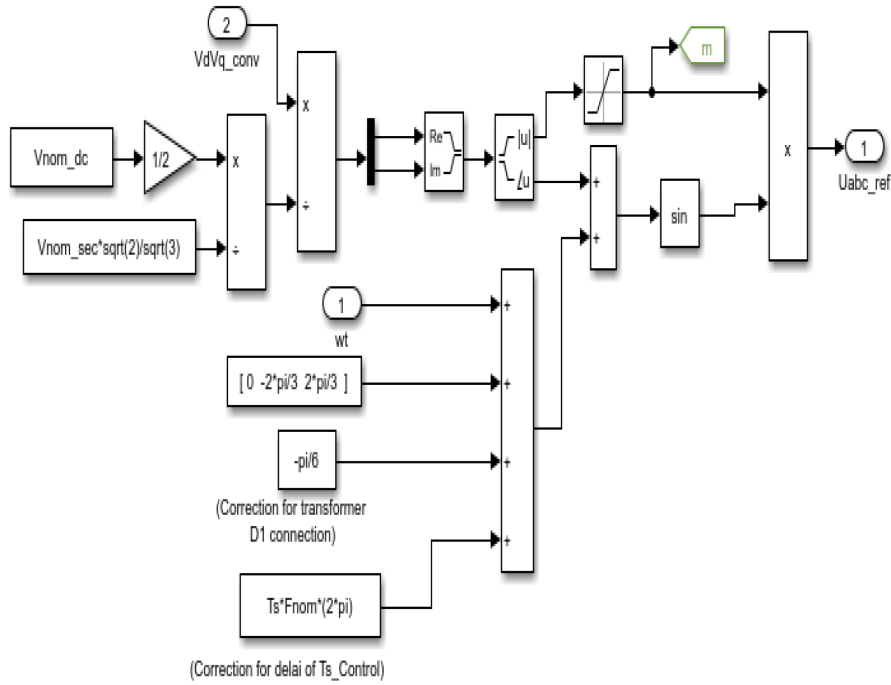


Fig. 9.  $U_{ref-abc}$  generation.

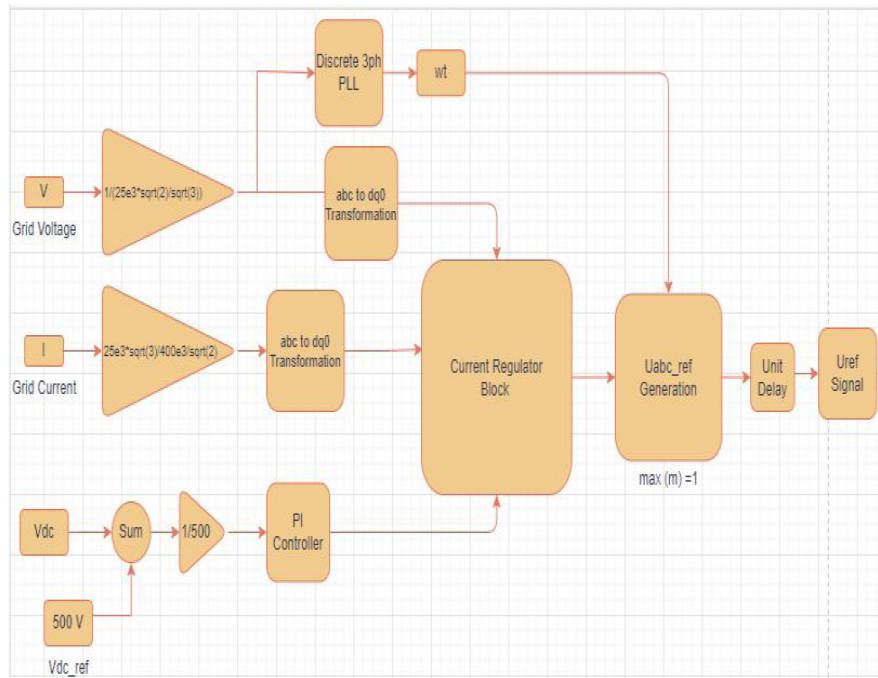


Fig. 10. Control diagram.

**A. Boost Converter's Performance**

Four separate boost converters were used for the four PV panels. In Fig. 12, it is clear that the application of the P&O MPPT technique

under PSC brings out the best results among all other conditions. The peak value of DC current without PSC and with P&O is 377.34 A, which dropped when the P&O algorithm was taken out from the

**TABLE III.**  
 INVERTER PARAMETERS

Number of bridge arms	3
Power electronic device	Average-model based VSC
Voltage	200 V

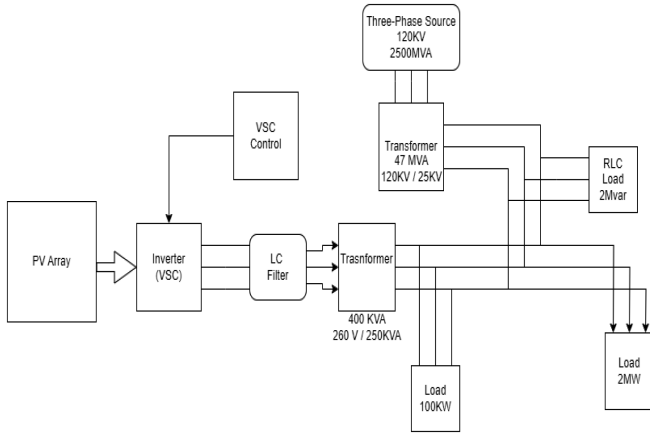


**Fig. 11.** Power diagram of grid-connected PV array.

MPPT controller. It is noticeable that under PSC, applying the P&O algorithm increased the overall current production from the PV panels. Fig. 13 represents similar characteristics of power extraction, just like the current production under the four conditions. In Fig. 14, under uniform shading conditions (without PSC), applying the P&O MPPT technique enabled the production of comparatively higher voltage from the PV panels. Under the PSC, higher voltages were extracted by the application of the MPPT technique.

**B. Performance of the Voltage Source Inverter**

The grid voltage in all conditions: Fig. 15 shows the grid voltage’s steady-state response. Notably, there are no ripple components visible in the waveforms, and they remain in phase.

Fig. 16 demonstrates the present waveforms resulting from the electric grid’s operating at unity power factor using the P&O algorithm under PSC. The peak current injected into the grid varies with different irradiances while maintaining a consistent phase and a power factor of unity. Consequently, grid voltage and current show minimal ripple. Fig. 17 also illustrates the same but without the application of any MPPT technique. Under no PSC, Fig. 18 displays the grid current waveform with the P&O algorithm applied, where the peak current is 12.38 A, whereas in Fig. 19, the peak value is 11.52 A without the algorithm applied.

Fig. 20 demonstrates the power generation that is being fed into the grid in all four conditions. Here, the reactive power in the steady-state condition is 0. Under PSC, the most peak power was generated by applying the P&O MPPT technique (peak value 376.62 kW). Under no PSC, the most power was also generated with the P&O MPPT technique (376.48 kW).

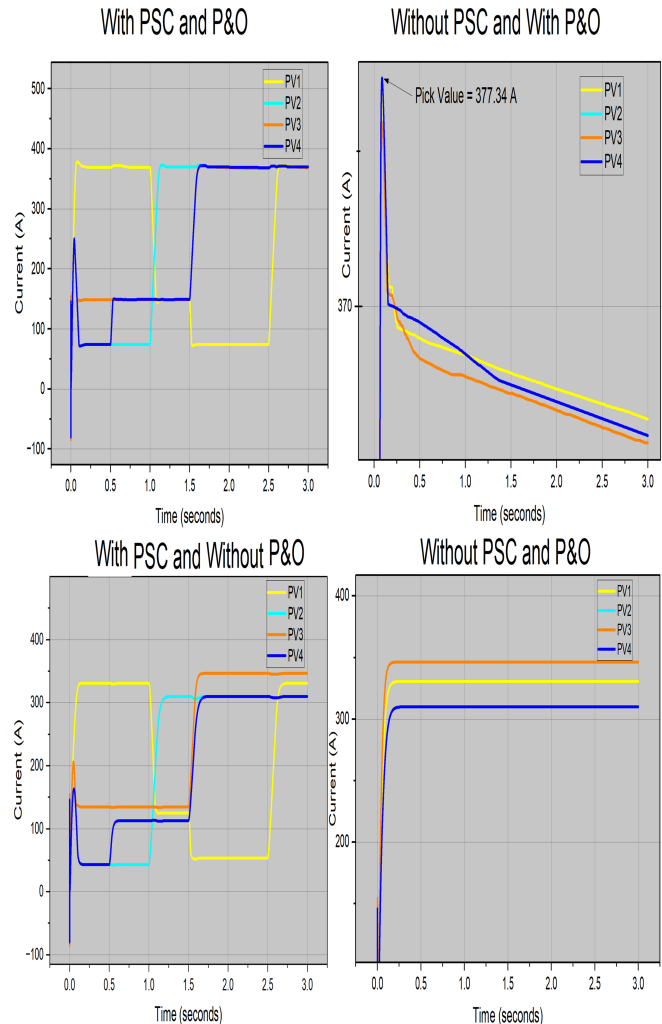


**Fig. 12.** Current in all conditions.

**C. Table of Grid Power for All Four Conditions**

The Table IV. presents an overview of the grid power behavior under four different conditions: with and without PSC, and with and without the P&O MPPT. The grid power values in the table range from 0.25 to 3.00 seconds, with a consistent time delay of 0.25 seconds. Under PSC, the grid power exhibits a gradual increase over time. In contrast, without PSC, the grid power remains relatively stable. The influence of the P&O MPPT on grid power is not readily apparent from the table. However, it is noteworthy that the grid power reaches its peak sooner in the absence of PSC compared to the other conditions.

For all conditions, input power is 400 kW.

**D. Efficiency of Grid Power**

Without PSC and with P&O:

Peak value = 376.48 kW.

Efficiency = (output power/input power) \* 100% = (376.48/400)\*100% = 94.12%.

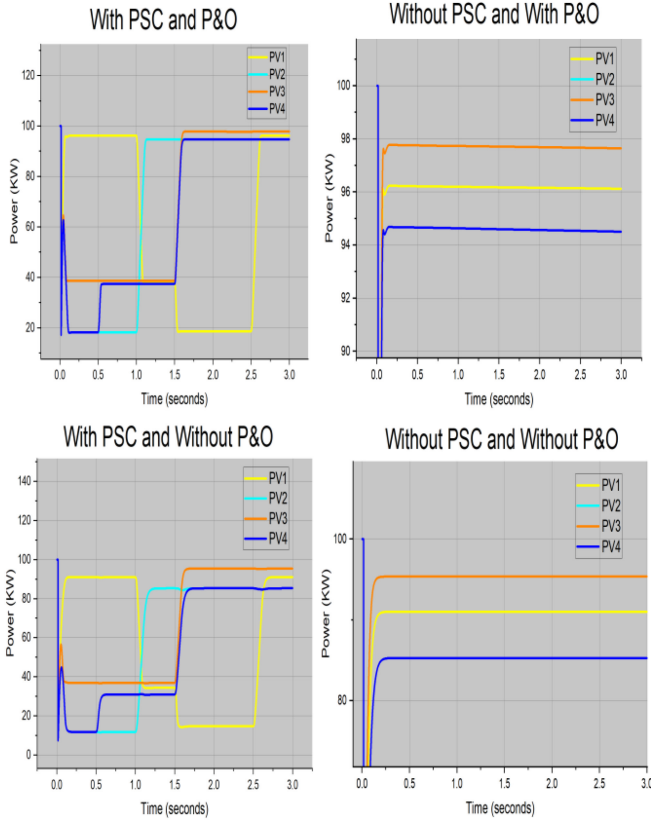


Fig. 13. Power in all conditions.

With PSC and with P&O:

Peak value = 351.17 kW.

Efficiency = (output power/input power)\* 100% = 87.8%.

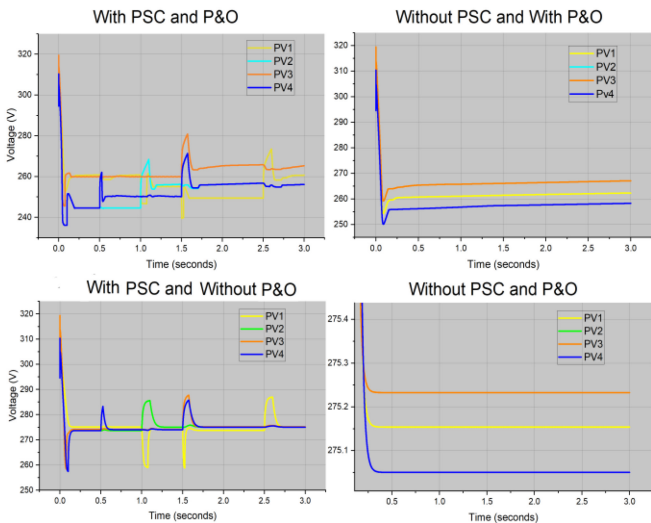


Fig. 14. Voltage in all conditions.

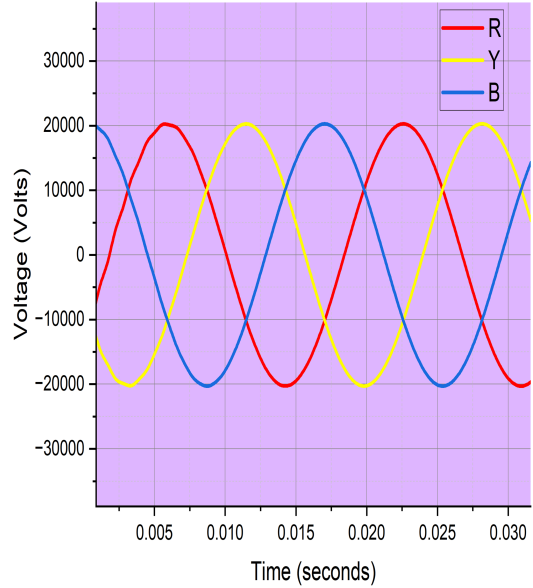


Fig. 15. Steady-state response of grid voltage.

It can be observed from the calculations that the differences in power efficiency are primarily due to the presence of the P&O algorithm. If P&O is applied, the efficiency is higher; otherwise, without P&O, the efficiency is quite lower.

Difference of power efficiency = (94.12 – 87.8) = 7.32%.

**E. THD Comparison of the VSI in Four Different Situations**

Through improved RLC filter design and a higher switching frequency, the system achieved enhanced performance. The grid current and voltage THD frequency spectra for all four conditions are shown in Figs. 21-24, ranging from 20 to 100 Hz.

As depicted in the graph, the THD of the grid current varies significantly depending on the presence or absence of PSC on the PV array. When PSC is not present, the THD of the grid current is notably lower compared to scenarios with PSC. While incorporating a P&O MPPT algorithm can slightly reduce THD, the most dramatic impact on THD is observed by simply eliminating or introducing PSC within the system.

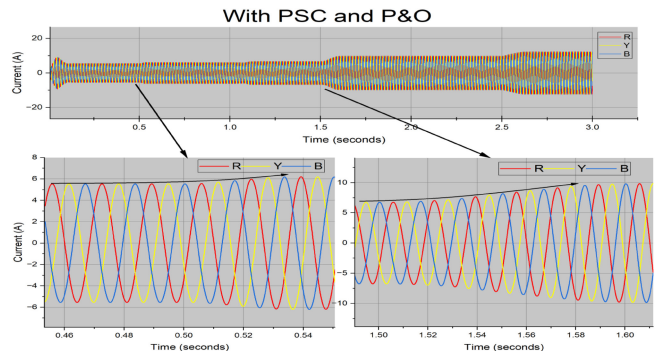


Fig. 16. Grid current waveform with PSC and with P&O.

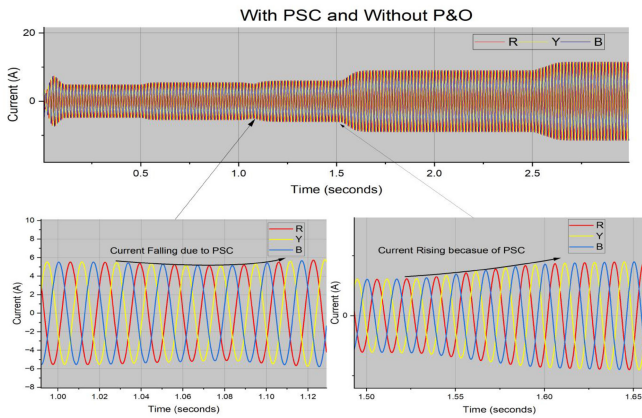


Fig. 17 Grid current waveform with PSC and without P&O.

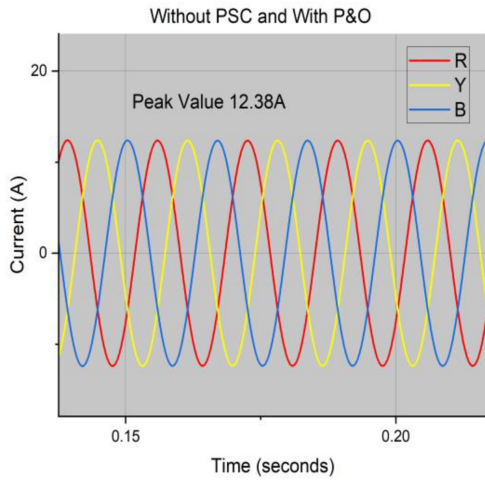


Fig. 18. Grid current waveform without PSC and with P&O.

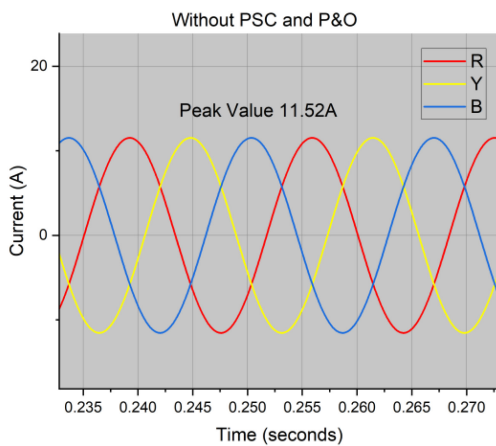


Fig. 19. Grid current waveform without PSC and P&O.

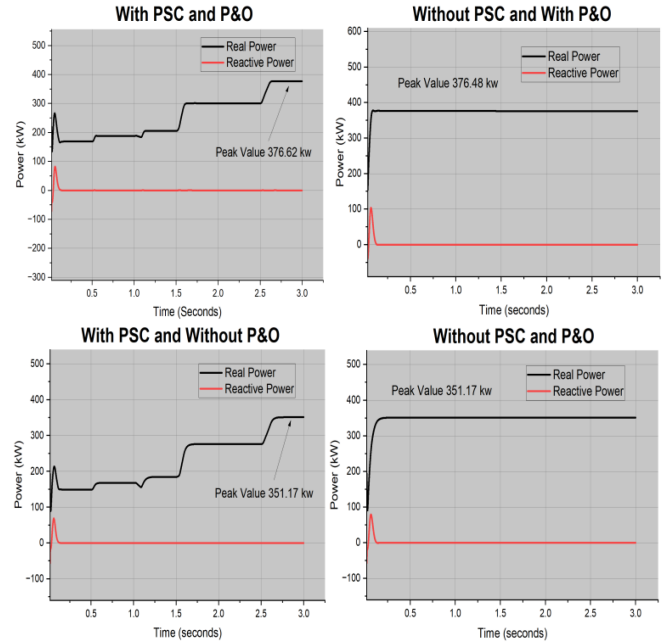


Fig. 20. Power generation in all conditions (GRID).

For the grid voltage THD, all four conditions show almost similar values of THD (%). Fig. 25 illustrates the THD of the grid voltage spectrum, focusing on the frequency range from 20 to 100 Hz.

Figs. 26 and 27 present bar graphs illustrating the THD percentages for grid current and voltage, respectively. A significant disparity

TABLE IV.  
 GRID POWER FOR ALL FOUR CONDITIONS

Time (seconds)	Power (kW)			
	With PSC and P&O	With PSC and without P&O	Without PSC and with P&O	Without PSC and P&O
0.25	168.632	149.093	376.626	350.996
0.50	168.622	149.095	376.552	351.171
0.75	187.540	168.025	376.497	351.171
1.00	187.509	168.026	376.458	351.171
1.25	205.496	184.548	376.405	351.171
1.50	205.482	184.704	376.351	351.171
1.75	300.553	276.194	376.307	351.171
2.00	300.564	276.289	376.262	351.171
2.25	300.520	276.289	376.213	351.171
2.50	300.481	276.289	376.166	351.171
2.75	376.701	351.073	376.120	351.171
3.00	376.566	351.171	376.064	351.171

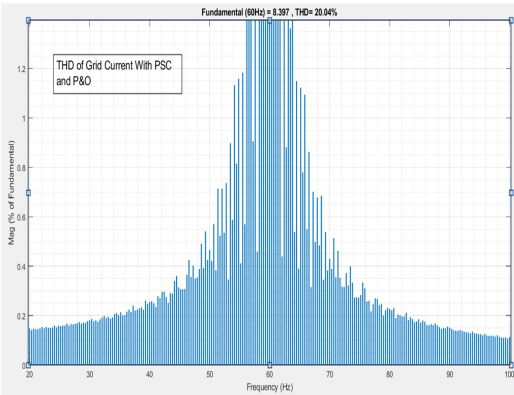


Fig. 21. THD of grid current with PSC and P&O.

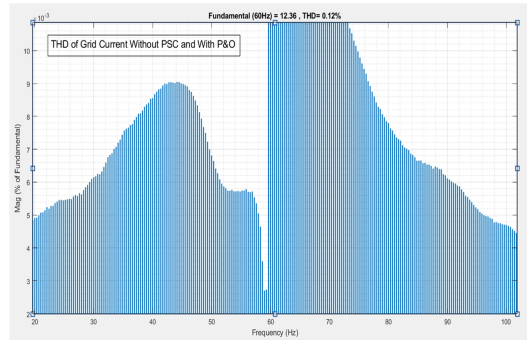


Fig. 23. THD of grid current without PSC and with P&O.

in THD is evident for the three-phase grid current. Without PSC, the THD values are considerably lower compared to scenarios with PSC. While the P&O MPPT algorithm can marginally reduce THD, the primary factor influencing THD remains the presence or absence of PSC. In contrast, the THD values for the three-phase grid voltage (phases R, Y, and B) are consistently low, ranging from 0.06% to 0.07%. Notably, when PSC is absent, the THD for grid voltage approaches 0.

a PV system. Key metrics such as grid current, PV voltage, PV current, PV power, and THD are impacted by the PSC.

Regarding grid power, it was observed that a system without a PSC exhibited stable power output, reaching its peak value rapidly. In terms of THD, removing the PSC led to a notable reduction in its

In this study, an analysis has been conducted to observe the impact of PSC on a grid-integrated PV system. The traditional P&O method has been employed as the MPPT technique, and a PSC has been induced. Some different conditions combining the MPPT algorithm and PSC have been utilized to demonstrate the impact of changing shading conditions on the power generation of the grid-connected PV system. In conclusion, a comprehensive simulation is conducted that takes into account the entirety of the system, comprising both the PV generator and the three-phase voltage source inverter with a thorough and careful focus on inverter modeling, emerges as a robust and viable approach for accurately predicting the energy production of the entire facility when it is interconnected with the utility grid. The presence of PSC significantly influences the performance of

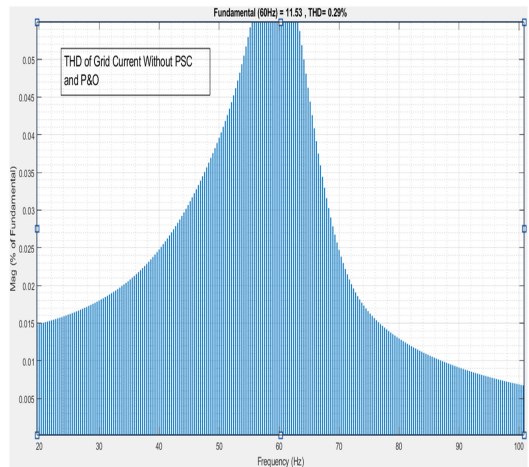


Fig. 24. THD of grid current without PSC and P&O.

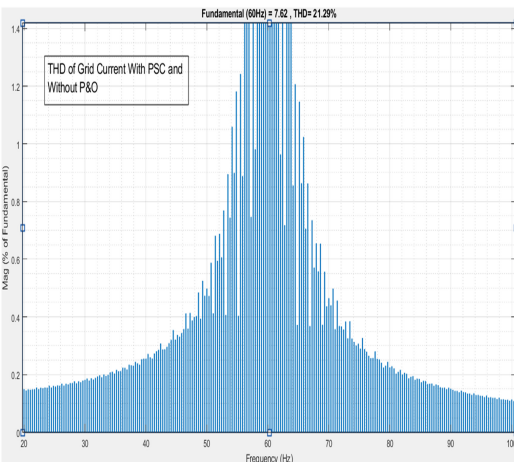


Fig. 22. THD of grid current with PSC and without P&O.

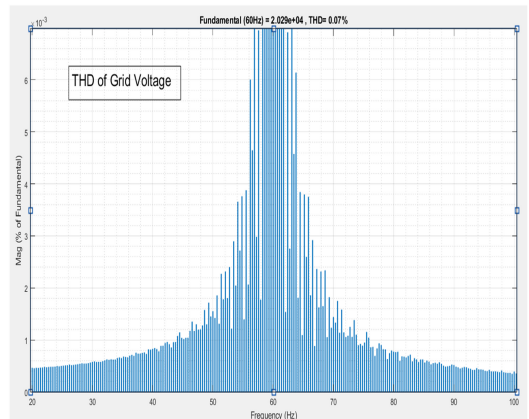


Fig. 25. THD of grid voltage.

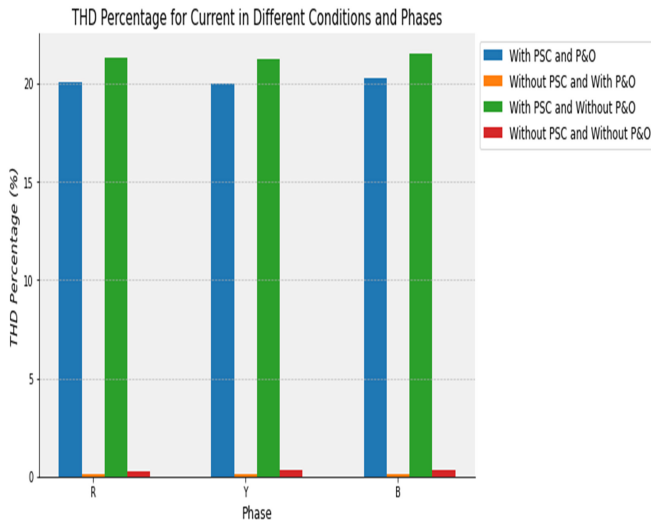


Fig. 26. Bar chart of THD (%) for grid current.

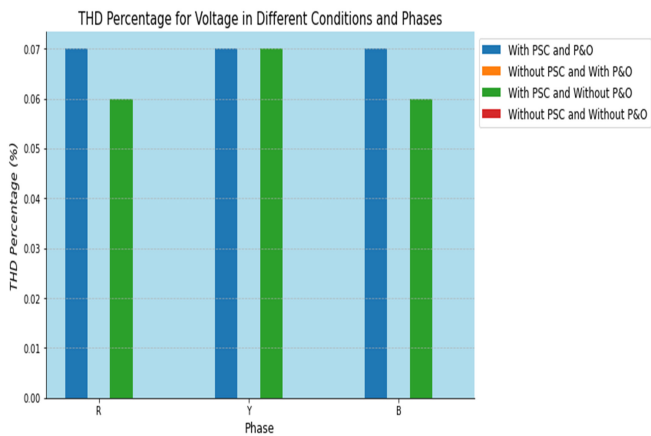


Fig. 27. Bar chart of THD (%) for grid voltage.

value. Additionally, the grid power efficiency demonstrated an improvement in the absence of the PSC.

Furthermore, the peak value of grid current was lower when the system operated without a P&O MPPT algorithm.

**Availability of Data and Materials:** The data that support the findings of this study are available on request from the corresponding author.

**Peer-review:** Externally peer-reviewed.

**Author Contributions:** Concept – A.A., M.J.B.; Design – F.R.; Supervision – A.A.; Resources – M.J.B., F.R.; Materials – A.A., F.R., M.J.B.; Data Collection and/or Processing – F.R.; Analysis and/or Interpretation – M.J.B., F.R.; Literature Search – M.J.B.; Writing – M.J.B., F.R., M.Y.; Critical Review – A.A., M.J.B.

**Declaration of Interests:** The authors have no conflicts of interest to declare.

**Funding:** The authors declare that this study received no financial support.

## REFERENCES

1. M. Nurunnabi, N. K. Roy, and H. R. Pota, "Optimal sizing of grid-tied hybrid renewable energy systems considering inverter to pv ratio—A case study," *J. Renew. Sustain. Energy*, vol. 11, no. 1, 2019. [CrossRef]
2. A. Zakaria, F. B. Ismail, M. S. H. Lipu, and M. A. Hannan, "Uncertainty models for stochastic optimization in renewable energy applications," *Renew. Energy*, vol. 145, pp. 1543–1571, 2020. [CrossRef]
3. T. Fatima, U. Shahzad, and L. Cui, "Renewable and nonrenewable energy consumption, trade and CO<sub>2</sub> emissions in high emitter countries: Does the income level matter?," *J. Environ. Plan. Manag.*, vol. 64, no. 7, pp. 1227–1251, 2021. [CrossRef]
4. N. Fulghum, "Yearly electricity data," 2024, Ember. Available: emberclimate.org/data-catalogue/yearly-electricity-data/.
5. A. Ibrahim, R. Aboelsaud, and S. Obukhov, "Comprehensive analysis of pso and p&o for the global maximum power point tracking of the pv under partial shading," in International Youth Conference on Radio Electronics, Electrical and Power Engineering (REEPE). IEEE Publications, pp. 1–6, 2019. [CrossRef]
6. M. Brenna, F. Foiadelli, M. Longo, and D. Zaninelli, "Energy storage control for dispatching photovoltaic power," *IEEE Trans. Smart Grid*, vol. 9, no. 4, pp. 2419–2428, 2016. [CrossRef]
7. N. Karami, N. Moubayed, and R. Outbib, "General review and classification of different mppt techniques," *Renew. Sustain. Energy Rev.*, vol. 68, pp. 1–18, 2017. [CrossRef]
8. S. Kumar, and B. Singh, "A multipurpose pv system integrated to a three-phase distribution system using an lwdf-based approach," *IEEE Trans. Power Electron.*, vol. 33, no. 1, pp. 739–748, 2017. [CrossRef]
9. S. P. Energy, "Technology roadmap," tech. rep., Technical Report, IEA, 2014. Available online: <https://www.iea.org/reports/technology-roadmap-solar-photovoltaic-energy-2014>. pp. 5-21, 2014.
10. C. Li, "Unstable operation of photovoltaic inverter from field experiences," *IEEE Trans. Power Deliv.*, vol. 33, no. 2, pp. 1013–1015, 2017. [CrossRef]
11. X. Xie, Y. Zhan, H. Liu, W. Li, and C. Wu, "Wide-area monitoring and early-warning of subsynchronous oscillation in power systems with high-penetration of renewables," *Int. J. Electr. Power Energy Syst.*, vol. 108, pp. 31–39, 2019. [CrossRef]
12. Y. Zhao, Z. Yang, Y. Wang, and Y. Zhang, "Mechanism analysis of pcc harmonic resonance based on nonlinear self-oscillation concept in a high-power grid-tied photovoltaic plant," *Appl. Sci.*, vol. 8, no. 9, p. 1507, 2018. [CrossRef]
13. B. B. Taya, A. Ahammad, and F. I. Jahin, "Total harmonic distortion mitigation and voltage control using distribution static synchronous compensator and hybrid active power filter," *IJATEE*, vol. 11, no. 114, pp. 624–643, 2024. [CrossRef]
14. M. Lei et al., "An mpc-based ess control method for pv power smoothing applications," *IEEE Trans. Power Electron.*, vol. 33, no. 3, pp. 2136–2144, 2017. [CrossRef]
15. S. Kumar, and B. Singh, "A multipurpose pv system integrated to a three-phase distribution system using an lwdf-based approach," *IEEE Trans. Power Electron.*, vol. 33, no. 1, pp. 739–748, 2017. [CrossRef]
16. M. M. Rahman, R. Abdullah, A. Ahammad, and I. K. Amin, "Performance analysis of LLC resonant and pulse width modulation direct current-direct current converters for buck and boost operation," *Turk J. Electr. Power Energy Syst.*, vol. 4, no. 2, pp. 96–107, 2024. [CrossRef]
17. M. A. Farahat, M. A. Enany, and A. Nasr, "Assessment of maximum power point tracking techniques for photovoltaic system applications," *J. Renew. Sustain. Energy*, vol. 7, no. 4, 2015. [CrossRef]
18. D. P. Hohm, and M. E. Ropp, "Comparative study of maximum power point tracking algorithms," *Prog. Photovolt. Res. Appl.*, vol. 11, no. 1, pp. 47–62, 2003. [CrossRef]

19. S. M. Amin, and B. F. Wollenberg, "Toward a smart grid: Power delivery for the 21st century," *IEEE Power Energy Mag.*, vol. 3, no. 5, pp. 34–41, 2005. [\[CrossRef\]](#)
20. R. Gupta, and G. Dyanamina, "MATLAB Simulation of Advanced MPPT Algorithm for Solar photovoltaic System," 2019, *Innovations in Power and Advanced Computing Technologies*. Vellore, India, 2019, pp. 1–7. [\[CrossRef\]](#)
21. M. Ahmed, M. Abdelrahem, and R. Kennel, "Highly efficient and robust grid connected photovoltaic system based model predictive control with kalman filtering capability," *Sustainability*, vol. 12, no. 11, p. 4542, 2020. [\[CrossRef\]](#)
22. M. Farhat, M. Hussein, and A. Atallah, "Advanced control strategies for performance improvement of a three phase grid connected photovoltaic system based on ga and pso techniques," *Engineering Research Journal (ERJ)*, vol. 2, pp. 81–88, 2018. Journal Homepage: [www.fengbu.edu.eg](http://www.fengbu.edu.eg)